Maximum Credible Earthquake Ground Motions with Focus on Site Amplification due to Deep Subsurface

Takashi Nagao
Research Center for Urban Safety and Security
Kobe University
Kobe City, Japan
nagao@people.kobe-u.ac.jp

Abstract-Since an Earthquake Ground Motion (EGM) is amplified from the propagation through the ground, different models are required for each ground type in the seismic design of structures. While the shallow subsurface indicators are used for the classification of ground types, a deep subsurface has a significant impact on the amplification of the EGMs. This study discusses the maximum credible EGMs for seismic design reflecting seismic amplification due to deep subsurface. The design spectra, reflecting the site amplification factor of the target location, are presented by the calculation of the EGMs with the same source and path characteristics and different site amplification factors as recent major Japanese earthquake records have shown, from the perspective of establishing the maximum credible EGMs that may occur in the future at a target site. The present design spectra, which are based on the natural period of a shallow subsurface, are compared with those based on the site amplification factors, considering the effect of deep subsurfaces. Although there are almost no differences in the design spectra with the present design methods according to the surface ground type, the proposed method provides significantly different design spectra for each site amplification factor.

Keywords-maximum credible earthquake ground motion; site amplification factor; deep subsurface; earthquake response analysis

I. INTRODUCTION

Earthquake Ground Motions (EGMs) for seismic design are classified into two categories: moderate EGMs and Maximum Credible EGMs (MCEGMs). The former is used for the assessment of structural serviceability and the latter is used for the assessment of structural safety. MCEGMs are evaluated successfully by adequately taking into account source, path, and site amplification characteristics. A state-of-the-art method is highly applicable to the evaluation of MCEGMs because the said characteristics can be properly considered [1]. However, the application of the state-of-the-art method is often challenging and expensive in practical design. MCEGMs of seismic design codes [2–7] are determined by considering the seismicity and seismic amplification characteristic at the target site, however, conventional methods employed in seismic design codes have been pointed out to overestimate or underestimate MCEGMs at many sites due to the insufficient consideration of source, path, and site amplification characterisitics [1]. Of the three characteristics, site amplification characteristic is known to greatly differ from place to place, thereby precise evaluation of the site amplification characteristic is of utmost importance for MCEGMs. The problem of the conventional methods for the evaluation of site amplification characteristic is that the methods only consider seismic amplification factor by shallow subsurface. The ground comprises of both shallow and deep subsurfaces. The boundary between the two is the engineering bedrock. It has high rigidity and a negligible nonlinear response during major earthquake events. Seismic amplification factors by a deep subsurface are significantly larger than those by a shallow subsurface. Therefore, considering amplification factors due to shallow subsurface alone significantly underestimates the site amplification factors [1, 8–10].

To evaluate the site amplification characteristics of a deep subsurface, various methods utilizing the strong-motion record have been proposed. The spectral ratio of the horizontal component of the target site to the reference site (Standard Spectral Ratio-SSR) [11] and the spectral ratio of the horizontal component to the vertical component at the target site (Receiver Function Method-RF) [12] are taken as examples of the simplified method. Another method is the spectral inversion which separates the source, path, and site characteristics from the earthquake record observed at multiple sites [13–15]. These differences in the evaluation methods of site amplification factors result in variations in the calculated amplification factors. Comparative studies of the differences between these techniques [16–20] have revealed that the spectral inversion method and the SSR method produce almost the same amplitude, while the RF method results in lower amplitude compared with other approaches. It should be noted that the SSR method requires a hard-rock site as a reference location that is in close proximity to the target site. However, identifying the ideal reference site is not always possible, especially at sedimentary sites. Furthermore, surface-rock sites have their specific amplification because of the effects of near-surface weathering or cracking [21]. Consequently, the SSR method may result in an underestimation of the site amplification factor [8, 19].

Considering the above points, it could be said that the spectral inversion method is highly applicable for the precise evaluation of the site amplification factors for arbitrary sites.

Corresponding author: Takashi Nagao

This article discusses MCEGMs considering site-specific amplification factors obtained by spectral inversion, while conforming to the method for establishing the MCEGMs of the Japanese Specifications for Highway Bridges (JSHB) [7].

II. MCEGMS OF JSHB

A. MCEGMs of JSHB and their Problems

The JSHB stipulates six kinds of standard MCEGMs. These encompass two earthquake types (types 1 and 2) and three kinds of ground conditions (types 1, 2, and 3). A type 1 earthquake is the MCEGM from a large-scale inter-plate earthquake in the subduction area, while type 2 is the MCEGM from a shallow crustal earthquake. The type 1 MCEGMs were established considering EGM records, such as the 1923 Kanto Earthquake, the 2003 Tokachi-oki Earthquake, and the 2011 off the Pacific coast of Tohoku Earthquake. The type 2 MCEGMs were established mainly with reference to the EGM records from the 1995 Kobe Earthquake. The standard MCEGMs are multiplied by a regional coefficient in the range of 0.7–1.2 to reflect the seismicity of the site of interest. The ground condition is classified by the natural period of the shallow subsurface using the quarter-wavelength approximation:

$$T_G = 4\sum_{i=1}^{n}\frac{H_i}{V_{si}} \quad (1)$$

where T_G is the natural period of the shallow subsurface, and H_i and V_{si} are the thickness and the S-wave velocity of the i-th layer for the shallow subsurface respectively. The ground conditions are classified in accordance with the natural period of the site of interest as follows: type 1 when T_G is 0.2s or less, type 3 when T_G is 0.6s or more, and type 2 otherwise.

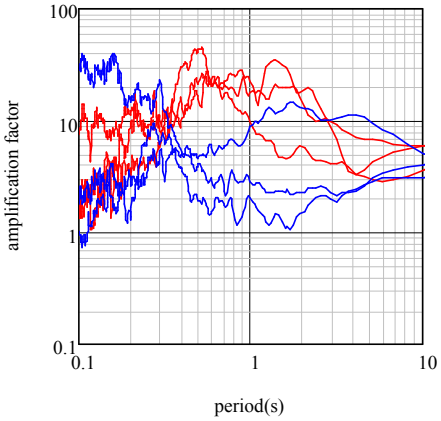

Fig. 1. Site amplification factor comparisons.

The importance of the amplification characteristics by deep subsurfaces is briefly demonstrated. Figure 1 shows the site amplification factors of three type 1 ground sites (ISKH01, MYZ017, and SZOH01) and three type 3 ground sites (KGWH01, TTR005, and YMT006) from strong-motion observation locations in the K-NET [22] and KiK-net [23] networks. The site amplification factor is the amplification magnitude from the seismic bedrock to the ground surface determined by the spectral inversion [24]. The red line expresses the type 1 ground, while the blue line denotes the type 3 ground. In the 0.6–1.0s period, the amplification factor of type 1 ground with a shallow subsurface natural period of 0.2s or less greatly exceeds the amplification factor of type 3 ground with a shallow subsurface natural period of 0.6s or more. In addition, the amplification factor of the type 1 ground exceeds that of the type 3 ground in the period up to 2.5s, except for MYZ017. This is caused by the differences in the amplification factor due to the deep subsurface. It is evident that the ground type classification of the JSHB is not appropriate.

B. Comparison of JSHB's MCEGMs and Recent Major EGMs

The intensity of the present MCEGMs of the JSHB was compared with recently recorded major EGMs. Three period bands of 0.2–0.6, 0.6–1.0, and 1.0–2.0s were defined by referring to the range of the natural periods of highway bridges with span lengths of 200m or less [7]. Then, records showing remarkably large spectral response acceleration in the above period ranges were extracted from recent major earthquake records. The focus was on the sites where the site amplification factor was calculated by spectral inversion [24].

TABLE I. TARGET SEISMIC WAVES

Period (s)	Earthquake	Station
0.2-0.6	2003 Tokachi-oki Earthquake	HKD086 (2)
	2004 Mid Niigata Prefecture Earthquake	NIG021 (1)
	2008 Iwate-Miyagi Nairiku Earthquake	AKTH04 (1)
	2011 off the Pacific coast of Tohoku Earthquake	IBR003 (1), IBRH11 (2)
	2016 Kumamoto Earthquake	KMMH16 (2)
0.6-1.0	1995 Southern Hyogo Prefecture Earthquake	Port Island (3)
	2000 Western Tottori Prefecture Earthquake	TTRH02 (1), TTR008 (3)
	2003 Tokachi-oki Earthquake	HKD086 (2)
	2004 Mid Niigata Prefecture Earthquake	NIG019 (1)
	2007Noto Hanto Earthquake	ISK005 (3)
	2008 Iwate-Miyagi Nairiku Earthquake	AKTH04 (1)
	2011 off the Pacific coast of Tohoku Earthquake	MYG013 (2)
	2018 Hokkaido Eastern Iburi Earthquake	HKD128 (2)
1.0-2.0	2000 Western Tottori Prefecture Earthquake	TTRH02 (1)
	2003 Tokachi-oki Earthquake	HKD086 (2), HKD098 (1)
	2004 Mid Niigata Prefecture Earthquake	NIG019 (1)
	2007 Niigataken Chuetsu-oki Earthquake	NIG018 (2)
	2011 off the Pacific coast of Tohoku Earthquake	MYG006 (2)

The selected seismic records are presented in Table I. The numbers in parentheses are the ground types according to the JSHB. By evaluating the ground types, it is evident that the K-NET site has the largest P-S logging data down to 20m below ground surface. Consequently, the ground conditions leading to the engineering bedrock are unknown and the ground types

cannot be determined at several locations. For those sites, the ground type was assessed with the following method. At first, it was assumed that the engineering bedrock with an S-wave velocity of 400m/s appears below the deepest point for which P-S logging data have been obtained and that no soil layer with an S-wave velocity exceeding 400m/s appears down to 30m below the ground surface. Next, in accordance with [25], average shear-wave velocity of the top 30m (*Vs*30) was estimated from the average S-wave velocity of less than 20m in the surface layer, and the ground structures from the deepest position of P-S logging to a depth of 30m were evaluated. The EGMs of the observation records in Table I were compared with the MCEGMs of the JSHB in Figure 2. The thin gray line represents the individual EGM, the solid blue line expresses the average, the broken blue line denotes the average and standard deviation EGM. The solid red, black, and green lines are the MCEGMs of ground types 1, 2, and 3 of the JSHB respectively. The damping constant was established at 5% of the standard value.

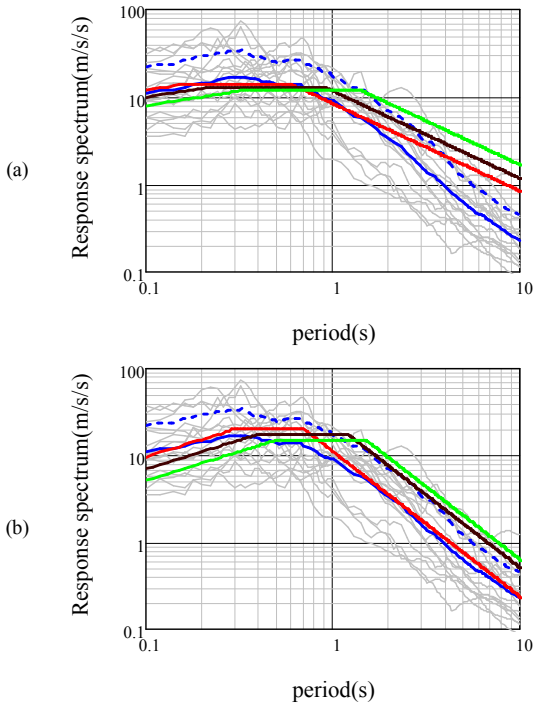

Fig. 2. Comparison of major earthquakes and design spectra: (a) type 1 EGM, (b) type 2 EGM.

From the comparison of the observed EGMs and the MCEGMs of the JSHB, the average of the observed spectra of recent major earthquakes in the period range of less than 1s and the average and standard deviation of the observed spectra in the period range of more than 1s were found to generally correspond to the MCEGMs of the JSHB. However, MCEGMs are not necessarily the largest observed EGMs, and the reference motions are selected from a statistical perspective. Furthermore, if the difference in levels due to the difference in the period bands is considered, it can be said that a highway bridge with a short natural period is a small-scale bridge with a relatively low degree of importance. Thus, an average level is regarded as reasonable, while a highway bridge with a long natural period is a long-span bridge with a high degree of importance, and an average and standard deviation level is assumed by engineering judgement. As different MCEGMs are established for different earthquake types, the variations in EGMs are compared according to the type of earthquakes in Figure 3. This research focuses on site-specific MCEGMs in terms of amplification. The specific type of earthquake is not considered, and the differences in EGMs between the interplate earthquakes and the crustal earthquakes are not remarkable. Therefore, the variations in earthquake types are not considered.

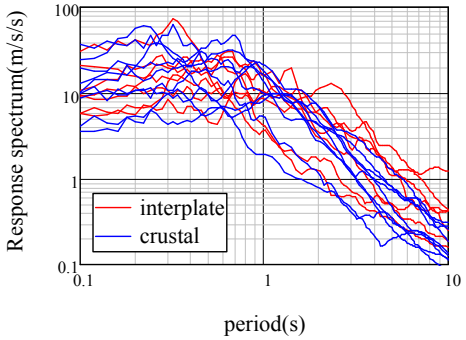

Fig. 3. Differences by earthquake type.

III. METHODS

A. Evaluation Methods of Site-Specific MCEGMs

As described above, the MCEGMs of the JSHB are established with reference to the records of past major earthquakes. This is because earthquakes of the same intensity as historic earthquake events may reoccur in any part of Japan in areas of high seismicity, and many earthquake records for reference in the assessment of MCEGMs have been accumulated. This paper discusses the MCEGMs considering site-specific amplification factors while conforming to the method for establishing the MCEGMs of JSHB. The EGM is determined by the characteristics of the source, path, and site amplification. The observed spectrum is represented by:

$$O(f) = S(f)\, P(f)\, G(f) \quad (2)$$

where $O(f)$ is the observed spectrum, $S(f)$ is the source spectrum, $P(f)$ is the path spectrum, $G(f)$ is the site amplification spectrum, and f is the frequency.

This study considers MCEGMs with the same source and path characteristics of past major earthquakes, and with the site amplification factor at the site of interest. The reference points from which seismograms are obtained are represented by subscript R, and the target sites are represented by subscript T. Thus, the seismic ground motion at the site to be examined is obtained by:

$$O_T(f) = O_R(f) \cdot \frac{G_T(f)}{G_R(f)} \quad (3)$$

During major earthquakes, shallow subsurfaces demonstrate nonlinearity. To consider the effect of this

nonlinearity, this study conducted an equivalent-linear earthquake response analysis considering the frequency dependency of the ground's nonlinear characteristics by [26] and evaluated an incident waveform at the engineering bedrock of the reference site. The obtained spectrum was divided by the site amplification factor $G_R(f)$ from the seismic bedrock to the engineering bedrock at the reference site and was multiplied by the site amplification factor $G_T(f)$ from the seismic bedrock to the engineering bedrock at the target site. Finally, an equivalent-linear earthquake response analysis was conducted to determine the $O_T(f)$ at the ground surface. The nonlinear characteristics of the soil used in the earthquake response analysis were taken from [27], while the site amplification factor from the seismic to the engineering bedrock was calculated by [24]. Since this amplification factor is the one from the ground surface to the seismic bedrock, the amplification factor from the ground surface to the engineering bedrock was eliminated by the application of the SH-wave multiple reflection theory.

B. Relationship between the Site Amplification Factor and the Response Spectrum

Figure 4 contains the site amplification factor, the acceleration Fourier amplitude spectrum, and the acceleration response spectrum of the seismic waveforms presented in Table I, extracting HKD098, NIG018, and TTR008 from ground type 1, 2, and 3 sites respectively. The acceleration Fourier amplitude spectrum was smoothed with the use of a Parzen window with a bandwidth of 0.2Hz. The peak frequencies of the Fourier spectrum and the site amplification factor do not necessarily correspond due to the influence of the nonlinearity of the shallow subsurface during strong earthquakes. However, both the Fourier amplitude and the response spectrum reveal a large value in the periodic band with a large site amplification factor in general. Therefore, when discussing the magnitude of the spectrum, the amplitude of the site amplification factor in the relevant periodic band must be considered.

C. Selection of Target Sites

A typical site amplification factor was selected from the following perspectives based on the nationwide site amplification factors determined by [24]. First, three period bands of 0.2–0.6, 0.6–1.0, and 1.0–2.0s were established. The nationwide site amplification factors were classified into large, medium, and small groups for these periodic zones. A total of 100 points were sampled from logarithmically spaced site amplification factors in a period of 0.1 to 10.0s, and Average Site Amplification Factors (ASAF) in the corresponding period bands were calculated. The frequency distributions of the ASAF for the respective bands are presented in Figure 5. The distribution of ASAF can be approximated to a lognormal distribution in every periodic band. The solid blue line in Figure 5 is the probability density function of the lognormal distribution. The cumulative distribution of ASAF was calculated by the lognormal distribution approximation, as shown in Figure 6. Since the distributions of 0.6–1.0 and 1.0–2.0s are very close to the mean and standard deviations, the cumulative distributions for the two bands almost overlap.

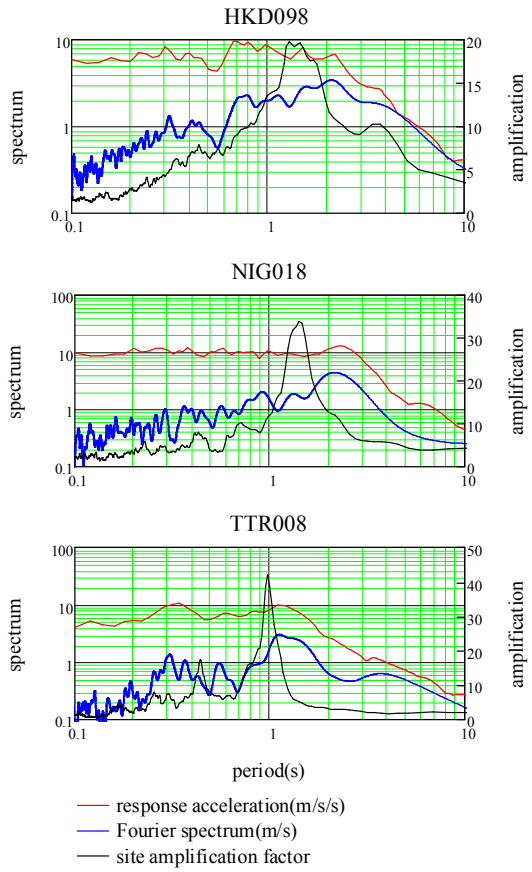

Fig. 4. Relationship between the site amplification factor, the Fourier spectrum, and the response spectrum.

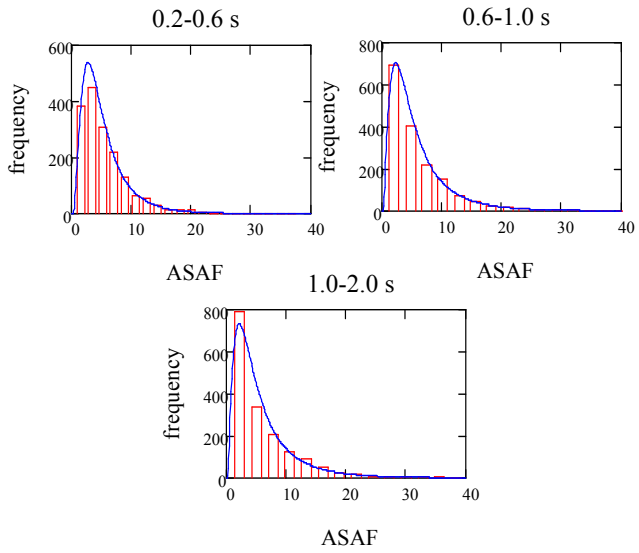

Fig. 5. ASAF frequency distributions.

Based on the results shown in Table II, the range of the cumulative distribution 0–1/3 is classified as the small site amplification factor. The range of 1/3–2/3 is classified as the medium site amplification factor, and the range 2/3–1 is

categorized as the large site amplification factor. Among the presented 1695 nationwide site amplification factor sites [24], 1067 are type 1 ground sites, 439 are type 2 sites, and 81 are type 3 sites. For each ground type, 3 sites were selected from the large, medium, and small ASAF in each periodic zone to eliminate the bias in the region. From this, a total of 81 sites, with 9 sites from each ground type and each periodic zone, were used as objects for the present study.

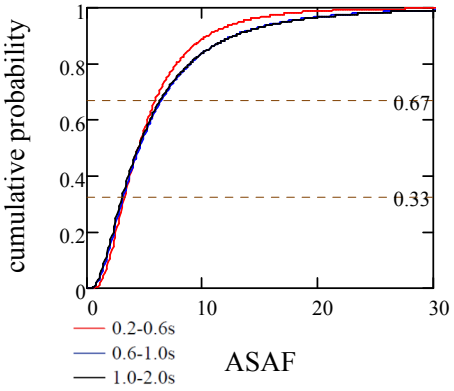

Fig. 6. ASAF cumulative distributions.

TABLE II. ASAF CLASSIFICATIONS

Period (s)	0.2–0.6	0.6–1.0	1.0–2.0
Small	ASAF < 3.30	ASAF < 3.19	ASAF < 3.08
Medium	3.30≤ASAF<5.88	3.19≤ASAF<6.39	3.08≤ASAF<6.30
Large	5.88 ≤ ASAF	6.39 ≤ ASAF	6.30 ≤ ASAF

TABLE III. TARGET SITES

	Type 1	Type 2	Type 3
0.2–0.6s			
small	GIFH24, KYT005, TKS011	CHBH14, MYG007, YMN011	CHB008, KSRH04, TTR005
medium	GNM007, HYG009, SMN006	KYT004, MYG013, NIG018	AKT015, HKD161, KYT002
large	IBUH06, KMM007, MYZ017	FKO015, ISK002, OITH07	ISK005, SBSH03, SZOH42
0.6–1.0s			
small	NGNH20, TCGH07, TTR003	HYGH11, IBRH11, OKY004	KGWH01, TTR005, YMT006
medium	AICH16, HKD134, SMN006	KOC002, TCGH16, WKY006	FKI003, KNG009, SRCH03
large	ISKH01, MYZ017, SZOH26	AOM024, KGS007, OIT016	IBUH03, ISK005, KYTH05
1.0–2.0s			
small	FKIH01, TCGH07, TTR003	AIC010, EHMH09, IWT004	AICH12, HYGH10, TTR005
medium	HKD057, KNG003, OIT007	KMM010, SZO025, TTRH04	FKIH05, ISK005, TTR008
large	ISK003, MYG005, SZOH26	KGS012, MYZ009, SZOH28	FKS020, IBUH03, KGSH07

Table III shows a list of the selected points. When the shallow subsurface P-S logging at the selected site did not reach the engineering bedrock, the subsurface structure was determined in the same manner described in the previous section. The site amplification factors of the selected sites are shown in Figure 7. The red, blue, and brown lines correspond to the large, medium, and small ASAF respectively.

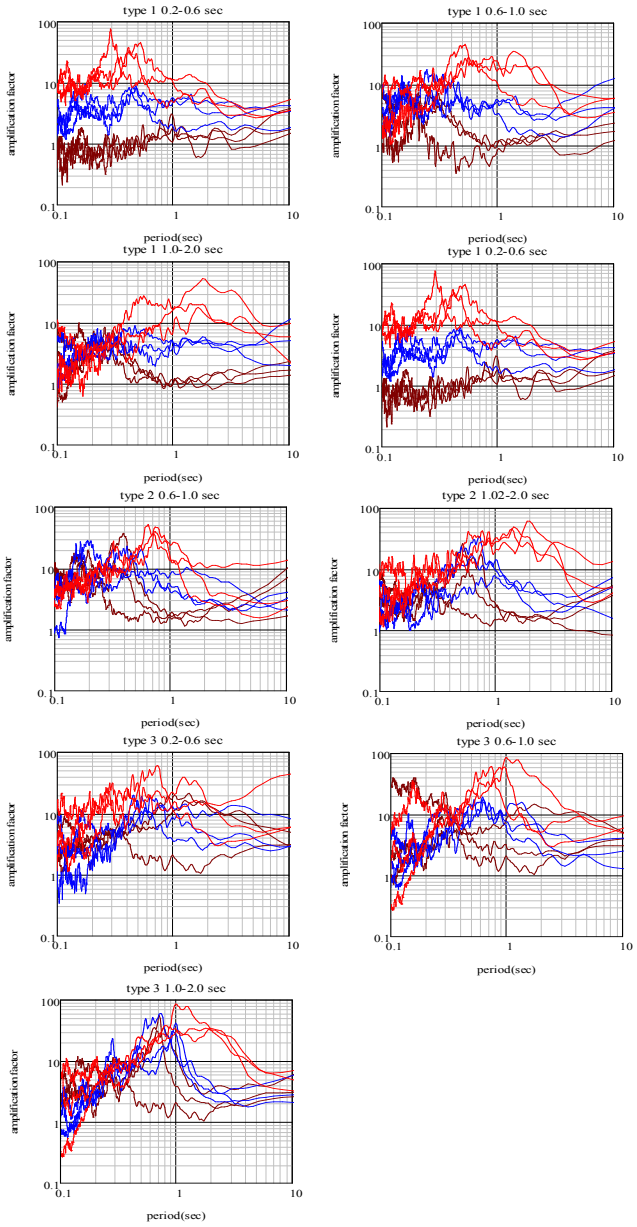

Fig. 7. Site amplification factor.

IV. RESULTS AND DISCUSSION

The 15 seismic waves shown in Table I are the reference EGMs. The sites' amplification factors were replaced, and the seismic ground motions were obtained at the 81 points shown in Table III. From this, a total of 1215 hypothetical EGMs were

acquired. Several sites are selected multiple times along with locations identical to the reference seismic ground motion observed sites in Table III. In this study, however, the statistical analyses focus on the period zone, ground type, and site amplification factor. Therefore, duplication is permitted with emphasis on the fact that the number of data is the same for each item. Figure 8 presents the results of a series of processes using the reference recording of the Noto Hanto Earthquake in 2007 at ISK005 and the target site KNG009 as examples. When a conventional equivalent-linear earthquake response analysis is conducted for a major earthquake, the amplification factor from the engineering bedrock to the ground surface tends to become significantly smaller than 1.0, especially in the high-frequency range, resulting in an underestimation of amplification. In such cases, the deconvolved EGM at the engineering bedrock becomes excessively large in amplitude, which generates unreliable results. This study conducted equivalent-linear earthquake response analyses, considering the frequency dependency of the nonlinear characteristics of the ground by [26], as described above, and no such phenomenon was observed.

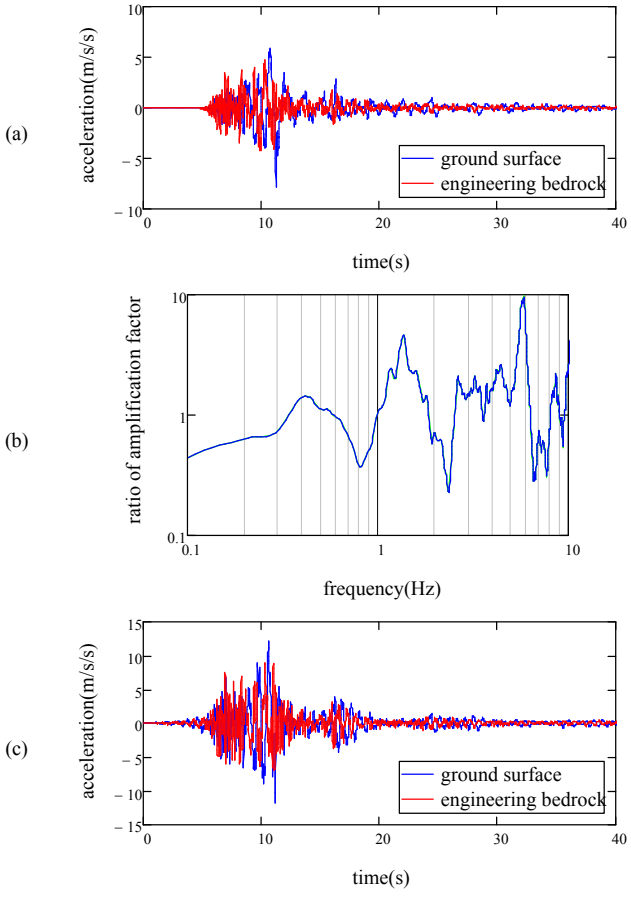

Fig. 8. Example of seismic ground motion calculation. (a) Deconvolution at ISK005, (b) ratio of amplification factor, (c) convolution at KNG009

The obtained acceleration response spectra for each ground type are shown in Figure 9. The thin gray line denotes the individual response spectrum, the bold red line expresses the logarithmic mean, and the bold blue line signifies the logarithmic mean and logarithmic standard deviation. Figure 10 displays the response spectra of the logarithmic mean and the logarithmic mean + logarithmic standard deviation for each ground type. The black, blue, and red lines correspond to ground types 1, 2, and 3, respectively, the solid lines represent the logarithmic mean + logarithmic standard deviation, and the broken lines are the logarithmic mean spectra.

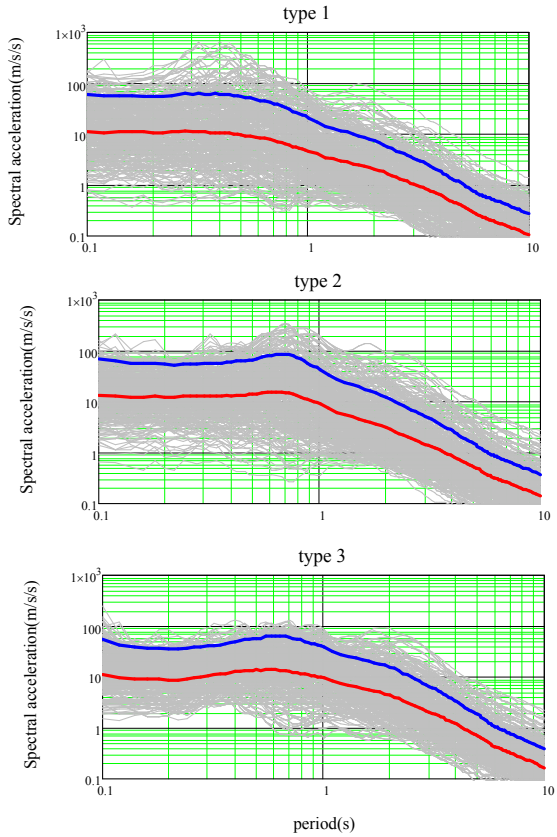

Fig. 9. Response spectrum (by ground type).

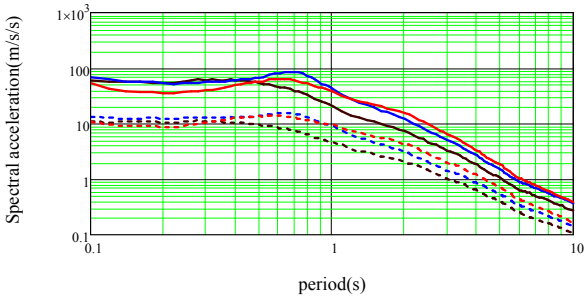

Fig. 10. Response spectrum (representative value).

Comparing the logarithmic mean and the logarithmic mean and logarithmic standard deviation response spectra, the type 1 ground spectra tend to be slightly smaller than the values of type 2 and 3 ground spectra in the frequency band of 0.5s or more. However, the difference is unremarkable. Comparing the

logarithmic mean and logarithmic standard deviation response spectra, the value of the type 3 ground tends to be slightly smaller in the periodic zone of 0.4s or less compared with the values of the types 1 and 2, but the difference is still unremarkable.

The obtained response spectra are shown in Figure 11 for large, medium, and small ASAF. The thin gray, bold red, and bold blue lines are the same as in Figure 8. Figure 12 presents the response spectra of the logarithmic mean and the logarithmic mean and logarithmic standard deviation spectra for each ASAF. The black, blue, and red lines are the small, medium, and large ASAF respectively. The solid line represents the logarithmic mean and logarithmic standard deviation, and the dashed line denotes the logarithmic mean spectra. According to the ASAF classification, the larger the ASAF, the larger the response spectra. For example, the values of the logarithmic mean and logarithmic standard deviation of the spectral response acceleration in a period of 1s are 80, 30, and 10m/s^2 in the order of large, medium, and small ASAF. A remarkable difference is observed. The same applies to the logarithmic mean spectra, where the magnitude of the ASAF and the magnitude of the response spectrum correspond. Thus, depending on the site, rational design spectra can be established by classifying the target site with the magnitude of the ASAF.

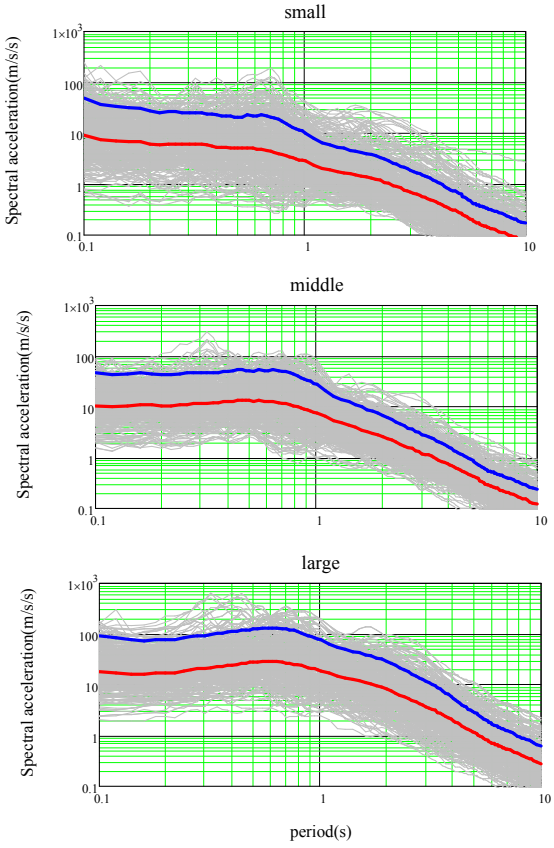

Fig. 11. Response spectrum (by ASAF)

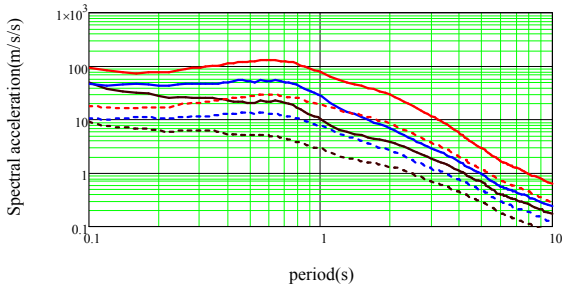

Fig. 12. Response spectrum (representative value)

Based on the results obtained, this study proposes design spectra according to the classification of ASAF. From the analysis of the present state of the design spectra in the JSHB, as described above, the proposed design spectra are the average spectra for the period range smaller than 1.0s and the average and standard deviation spectra for the period range larger than 1.0s. When the average spectrum and the average and standard deviation spectrum are combined in a period of 1s, spectral discontinuities occur. Therefore, the average spectrum of the short period side is extended in excess of 1s, and both are combined in a position corresponding with the average and standard deviation spectrum value. Finally, the function of the design spectrum is created to be the maximum envelope of the obtained result. Figure 13 contains the results along with the current design spectra.

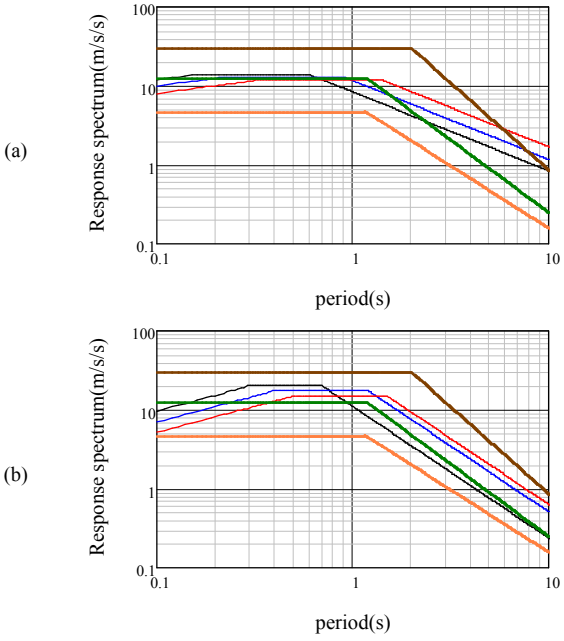

Fig. 13. Proposed spectrum: (a) Type 1 EGM, (b) Type 2 EGM

TABLE IV. PROPOSED SPECTRUM

ASAF	Spectral acceleration(m/s/s); S_0	
Small	$T < 1.2$; $S_0 = 6.0$	$1.2 \leqslant T$; $S_0 = 8 / T^{19/12}$
Medium	$T < 1.3$; $S_0 = 12.0$	$1.3 \leqslant T$; $S_0 = 18 / T^{5/3}$
Large	$T < 2.0$; $S_0 = 29.0$	$2.0 \leqslant T$; $S_0 = 133 / T^{11/5}$

T is the natural period (s)

In the diagram, the thick solid brown, green, and orange lines are the proposed spectra at the points where the ASAF is respectively large, medium, and small. The solid blue line is the spectrum of the mean and standard deviation, and the solid black, blue, and red lines are the design spectra of the current design methods of ground types 1, 2, and 3, respectively. When the proposed design spectrum and the present design spectrum are compared, the proposed spectrum coincides with the present design spectrum in the case of type 1 seismic motion in medium ASAF. It increases in the case of large ASAF and decreases in the case of small ASAF. Therefore, it can be said that a reasonable design can be conducted with the same construction cost as conventional national average costs. Regarding the type 2 EGM, in the present design spectra of all ground types in the period bands of less than 1s and of more than 1s, the present design spectra of ground types 2 and 3 are between those proposed for the middle and large ASAF. In terms of the national average cost, a more rational design can be produced while suppressing more the construction cost. The function of the proposed design spectrum is shown in Table IV.

V. CONCLUSION

From the perspective of establishing rational site-specific MCEGMs, this study proposed design spectra using ASAF as indices. The main obtained conclusions of this research are:

- From the comparison of the design spectra for the current level 2 EGMs with the spectra of recent strong-motion records of major earthquakes, it was found that the average spectra for a period of less than 1s and the average and standard deviation spectra for a period of more than 1s of recent major earthquakes generally correspond to the design spectra of the JSHB, which is the MCEGMs assumed at the construction site. It is presumed that this is based on engineering judgment that considers the importance of highway bridges.
- The response spectra of recent major earthquakes with different site amplification factors are evaluated by categorizing the ASAF period ranges as large, medium, and small. The design spectra corresponding to the mean and the mean and standard deviation are proposed for a period of less than 1s and a period of more than 1s respectively. From the comparison of the proposed spectrum with the current design spectrum, it becomes possible to conduct a rational design almost as economical as or slightly more economical than the present design method.

ACKNOWLEDGEMENTS

The authors would like to thank Yuta Kinoshita for helping in conducting the seismic response analysis. The ground structure data and the strong-motion observation records at K-NET and KiK-net sites were provided by the National Research Institute for Earth Science and Disaster Resilience.

REFERENCES

[1] T. Nagao and Y. Fukushima, "Source- and Site-Specific Earthquake Ground Motions:Application of a State-of-the-Art Evaluation Method," *Engineering, Technology & Applied Science Research*, vol. 10, no. 4, pp. 5882–5888, Aug. 2020, https://doi.org/10.48084/etasr.3612.

[2] *NEHRP recommended provisions for seismic regulations for new buildings and other structures*. Washington DC, USA: Building Seismic Safety Council for the Federal Emergency Management Agency, 2001.

[3] *AASHTO Guide Specifications for LRFD Seismic Bridge Design, 2nd Edition, with 2012 and 2014 Interim Revisions*. Washington, DC, USA: AASHTO, 2011.

[4] *Eurocode 8, Design of structures for earthquake resistance, Part1: general rules, seismic actions and rules for buildings*. Brussels, Belgium: European Committee for Standardization, 2003.

[5] *Recommended Provisions for Seismic Regulations for New Buildings and Other Structures (FEMA 450), Part 1: Provisions*. Washington DC, USA: Building Seismic Safety Council for the Federal Emergency Management Agency, 2003.

[6] *Minimum Design Loads for Buildings and Other Structures*, ASCE/SEI 7-10. ASCE, 2013, https://doi.org/10.1061/9780784412916.

[7] *Specifications for highway bridges, Part 5, Seismic design, ver. 2012*. Japan Road Association, 2016.

[8] D. M. Boore and W. B. Joyner, "Site amplifications for generic rock sites," *Bulletin of the Seismological Society of America*, vol. 87, no. 2, pp. 327–341, Apr. 1997.

[9] Y. Fukushima, T. Nagao, J. Oshige, and I. Suetomi, "Ground motion evaluation for intra-plate earthquake by different site amplification factors and source models," in *7th International Conference on Earthquake Geotechnical Engineering*, Roma, Italy, Jun. 2019, pp. 2484–2492.

[10] T. Nagao, "Seismic Amplification by Deep Subsurface and Proposal of a New Proxy," *Engineering, Technology & Applied Science Research*, vol. 10, no. 1, pp. 5157–5163, Feb. 2020, https://doi.org/10.48084/etasr.3276.

[11] R. D. Borcherdt, "Effects of local geology on ground motion near San Francisco Bay," *Bulletin of the Seismological Society of America*, vol. 60, no. 1, pp. 29–61, Feb. 1970.

[12] J. Lermo and F. J. Chávez-García, "Site effect evaluation using spectral ratios with only one station," *Bulletin of the Seismological Society of America*, vol. 83, no. 5, pp. 1574–1594, Oct. 1993.

[13] D. J. Andrews, "Objective Determination of Source Parameters and Similarity of Earthquakes of Different Size," in *Earthquake Source Mechanics*, Washington, USA: American Geophysical Union, 1986, pp. 259–267.

[14] T. Iwata and K. Irikura, "Source Parameters of the 1983 Japan Sea Earthquake Sequence," *Journal of Physics of the Earth*, vol. 36, no. 4, pp. 155–184, 1988, https://doi.org/10.4294/jpe1952.36.155.

[15] J. Boatwright, J. B. Fletcher, and T. E. Fumal, "A general inversion scheme for source, site, and propagation characteristics using multiply recorded sets of moderate-sized earthquakes," *Bulletin of the Seismological Society of America*, vol. 81, no. 5, pp. 1754–1782, Oct. 1991.

[16] L. F. Bonilla, J. H. Steidl, G. T. Lindley, A. G. Tumarkin, and R. J. Archuleta, "Site amplification in the San Fernando Valley, California: Variability of site-effect estimation using the S-wave, coda, and H/V methods," *Bulletin of the Seismological Society of America*, vol. 87, no. 3, pp. 710–730, Jun. 1997.

[17] E. H. Field and K. H. Jacob, "A comparison and test of various site-response estimation techniques, including three that are not reference-site dependent," *Bulletin of the Seismological Society of America*, vol. 85, no. 4, pp. 1127–1143, Aug. 1995.

[18] S. Parolai *et al.*, "Comparison of Different Site Response Estimation Techniques Using Aftershocks of the 1999 Izmit Earthquake," *Bulletin of the Seismological Society of America*, vol. 94, no. 3, pp. 1096–1108, Jun. 2004, https://doi.org/10.1785/0120030086.

[19] L. Malagnini, K. Mayeda, A. Akinci, and P. L. Bragato, "Estimating Absolute Site Effects," *Bulletin of the Seismological Society of America*, vol. 94, no. 4, pp. 1343–1352, Aug. 2004, https://doi.org/10.1785/012003161.

[20] S. Drouet, P. Triantafyllidis, A. Savvaidis, and N. Theodulidis, "Comparison of Site-Effects Estimation Methods Using the Lefkas, Greece, 2003 Earthquake Aftershocks," *Bulletin of the Seismological*

Society of America, vol. 98, no. 5, pp. 2349–2363, Oct. 2008, https://doi.org/10.1785/0120080004.

[21] J. H. Steidl, A. G. Tumarkin, and R. J. Archuleta, "What is a reference site?," *Bulletin of the Seismological Society of America*, vol. 86, no. 6, pp. 1733–1748, Dec. 1996.

[22] S. Kinoshita, "Kyoshin Net (K-NET)," *Seismological Research Letters*, vol. 69, no. 4, pp. 309–332, Jul. 1998, https://doi.org/10.1785/gssrl.69.4.309.

[23] S. Aoi, K. Obara, S. Hori, K. Kasahara, and Y. Okada, "New strong-motion observation network: KiK-net," *Eos, Transactions of the American Geophysical Union*, vol. 81, 2000.

[24] A. Nozu and T. Sugano, "Site Amplification Factor for Strong-Motion Sites in Northern Hokkaido, Japan, Based on Spectral Inversion Technique," Technical Note of the Port and Airport Research Institute, No.1102, 2005.

[25] D. M. Boore, E. M. Thompson, and H. Cadet, "Regional Correlations of VS30 and Velocities Averaged Over Depths Less Than and Greater Than 30 Meters," *Bulletin of the Seismological Society of America*, vol. 101, no. 6, pp. 3046–3059, Dec. 2011, https://doi.org/10.1785/0120110071.

[26] N. Yoshida, S. Kobayashi, I. Suetomi, and K. Miura, "Equivalent linear method considering frequency dependent characteristics of stiffness and damping," *Soil Dynamics and Earthquake Engineering*, vol. 22, no. 3, pp. 205–222, Apr. 2002, https://doi.org/10.1016/S0267-7261(02)00011-8.

[27] S. Yasuda and I. Yamaguchi, "Dynamic shear modules obtained in the laboratory and in-situ," in *Proceedings of the Symposium on Evaluation of Deformation and Strength of Sandy Grounds*, 1985, pp. 115–118.